

# Terawatt chirped pulse Raman amplified laser for two-color experiments

James C. Sanders,<sup>a,b,\*</sup> Rafal Zgadzaj,<sup>b</sup> and Michael C. Downer<sup>b</sup>

<sup>a</sup>Troy University, Department of Chemistry and Physics, Troy, Alabama, United States

<sup>b</sup>University of Texas at Austin, Department of Physics, Downer UT3 Lab,  
Austin, Texas, United States

**Abstract.** We report the generation of a two-color terawatt (TW) laser by the insertion of a three-stage barium nitrate Raman shifter and amplifier system into a conventional Ti:sapphire chirped-pulse amplification system. The Raman subsystem produces a pulse that is shifted from 800 to 873 nm and is amplified and compressed to TW scales (140 mJ and 140 fs) and then recombined with the 45-TW 800-nm fundamental pulse. © 2020 Society of Photo-Optical Instrumentation Engineers (SPIE) [DOI: [10.1117/1.OE.59.7.076110](https://doi.org/10.1117/1.OE.59.7.076110)]

**Keywords:** lasers; stimulated Raman scattering; nonlinear optics; laser amplifiers; Raman lasers.

Paper 20200511 received May 1, 2020; accepted for publication Jul. 6, 2020; published online Jul. 20, 2020.

## 1 Introduction

It is advantageous in some high-field experiments to accompany the main terawatt (TW) laser pulse ( $\sim 45$  TW, 800 nm) with a low-power,  $\sim 1$ -TW second pulse shifted in wavelength by  $\sim 50$  to 100 nm. Such a two-color laser system can be used for low walk-off velocity pump-probe experiments,<sup>1</sup> for amplification and compression of laser pulses inside a plasma,<sup>2,3</sup> or for control of laser-plasma instabilities such as relativistic self-focusing<sup>4-6</sup> and forward Raman scattering<sup>7</sup> inside a laser wakefield accelerator.<sup>8-10</sup> Frequency shifts of the desired magnitude cannot be produced by three-wave parametric processes because of IR absorption by the idler wave. To that end, Zavoronkov et al.<sup>11</sup> demonstrated the generation of 80- $\mu$ J, subgigawatt, 870-nm pulses by stimulated Raman scattering (SRS) of chirped 1.5-mJ, 800-nm pulses in barium nitrate; these pulses were recompressed to 190 fs. Grigsby et al.<sup>12</sup> reported the design and scaling of a chirped-pulse Raman amplified (CPRA) laser system to develop a 6-mJ laser, which was compressed to 110 fs and  $\sim 0.03$  TW and then synchronized with the main 5-TW Ti:sapphire laser system, and Guo et al.<sup>13</sup> have reported similar energy and duration.

In this paper, we report the scaling of a CPRA system to  $\sim$ TW, which results from a Raman-shifted laser with  $\sim 100$ -mJ and  $\sim 100$ -fs, bandwidth-limited pulses centered at 873 nm. This was achieved using a combined two-stage CPRA and a third amplifier stage consisting of a conventional multipass Ti:sapphire amplifier. Bandwidths of up to 20 nm FWHM and durations as short as 55 fs were observed, with sub-100 fs durations being routinely attainable. The Raman pulse was synchronized and recombined with the primary pulse of our laser system, and it was generated without substantially reducing the primary pulse energy. The Raman pulses generated are of sufficient power (and sufficiently short duration) to potentially be used as a “guide” laser to suppress relativistic self-focusing in dense plasmas as proposed by Kalmykov et al., which is a regime not yet achieved by previous CPRA experiments.

## 2 System Design

A variety of Raman-active media exist, but we chose barium nitrate,  $\text{Ba}(\text{NO}_3)_2$ , as our Raman shifting and gain medium. This choice was made in part because barium nitrate offers a relatively

---

\*Address all correspondence to James C. Sanders, E-mail: [jcsanders@troy.edu](mailto:jcsanders@troy.edu)

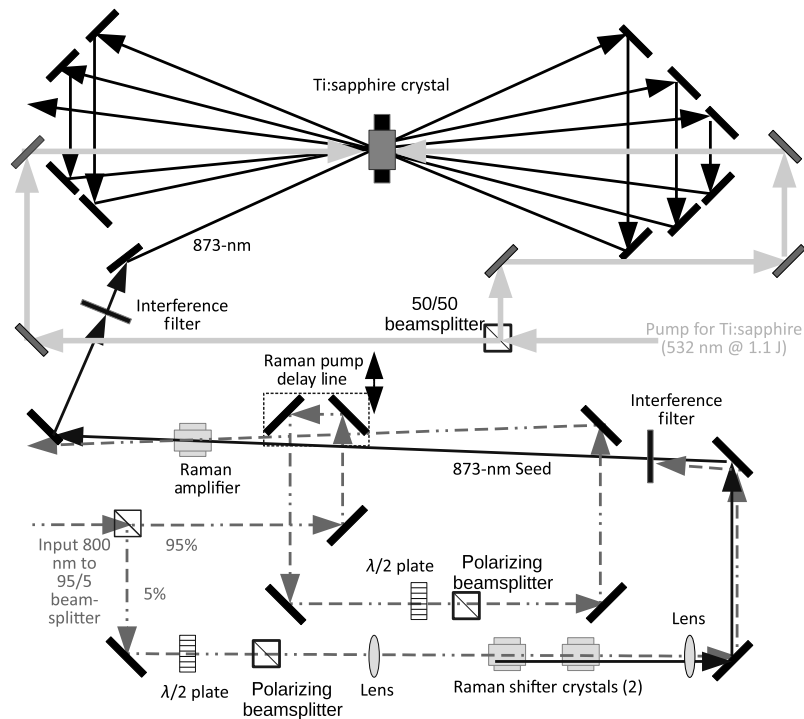


**Fig. 1** Details of the Raman shifter, the SRS amplifier, and the Ti:sapphire amplifier stages. The Raman pump and seed line energies are each independently adjusted using a half-wave plate and polarizing beamsplitter. The third-stage Ti:sapphire amplifier is set up in a six-pass bowtie configuration, and it is pumped by a frequency-doubled Nd:YAG laser.

large Raman gain in the stationary regime compared to other available solid-state Raman shifter media.<sup>14,15</sup> Some of the intended applications for this system require a larger spectral shift ( $\Delta\lambda > 70$  nm at 800 nm) than available from other solid-state sources, such as strontium molybdate ( $\Delta\lambda \sim 61$  nm at 800 nm), potassium gadolinium tungstate ( $\Delta\lambda \sim 62$  nm at 800 nm), or even strontium tungstate ( $\Delta\lambda \sim 64$  nm at 800 nm), to ensure a full spectral separation between the Raman-shifted pulse and the fundamental pulse. On the other hand, the Ti:sapphire amplifier system’s efficiency decreases substantially as the wavelength is moved from 800 to 900 nm, and so a second Stokes shift (926 nm) would yield a considerably smaller energy output. The  $\text{Ba}(\text{NO}_3)_2$  crystals used for this experiment were purchased from Marketch International, and they each have cross sections of 1 cm  $\times$  1 cm with length 5 cm.

Figure 1 shows the setup of the Raman shifter and amplifier lines, as well as the Ti:sapphire amplifier stage. The 50-mJ pulse is further split by a 95:5 beam splitter, with the smaller 2.5-mJ pulse being used to create a Raman seed line and the remaining pulse being sent to a Raman pump line, each of which may be independently attenuated using a half-wave plate and a polarizing beam splitter. The pulse in the Raman seed line is typically attenuated to  $\sim 0.5$  mJ and focused using an  $f/50$  and passes through a pair of  $\text{Ba}(\text{NO}_3)_2$  crystals, each of whose position may be independently adjusted to optimize Raman gain, mode quality, and bandwidth. Because barium nitrate is highly hygroscopic, each crystal is enclosed in a sealed aluminum holder, along with a desiccant material. The laser enters and exits the crystal’s enclosure through a pair of windows, which are oriented at the Brewster angle, to minimize reflections for both the 873-nm seed and the 800-nm pump.

Figure 2 shows how the Raman system is incorporated with the main CPA TW laser system. The main pulse—chirped to  $t = 500$  ps, centered at  $\lambda = 800$  nm, bandwidth  $\Delta\lambda = 40$  nm, and energy  $E = 1.8$  J—is split by a  $\sim 93:7$  beam splitter. The weaker pulse (split and attenuated to  $\sim 50$  mJ) is first shifted by Raman scattering to 873 nm, then amplified by SRS, and further amplified by a conventional six-pass, externally pumped Ti:sapphire amplifier to up to 300 mJ precompression. This is then compressed by a dedicated 1200 lines/mm diffraction grating pair

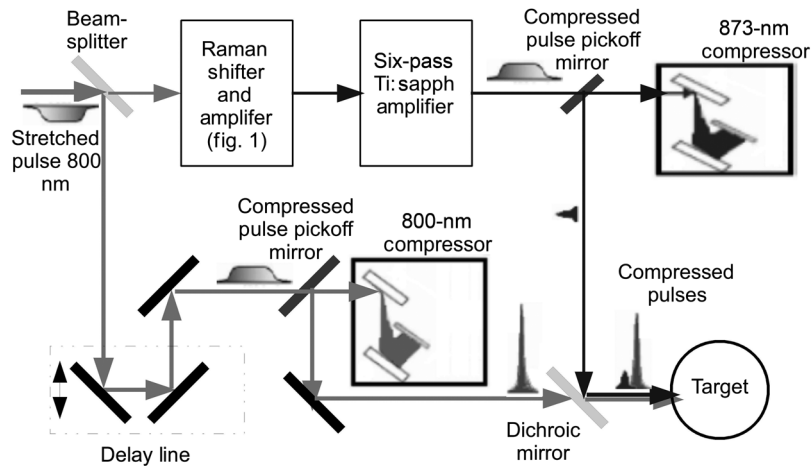


**Fig. 2** An overview of the 873-nm Raman generation from and its synchronization with the main 800-nm Ti:sapphire system. Note that the compressors each consist of a parallel grating pair and a rooftop mirror pair so that the output (compressed) beam exits parallel to but above the input (stretched) beam and so is picked off by a mirror positioned above the input beam.

to pulses of typical duration 140 fs and energy 140 mJ. The remaining energy is compressed in an 800-nm compressor (1480 lines/mm). A delay line is used to synchronize the main pulse with the Raman pulse.

The Raman pump line is typically attenuated to  $\sim 25$  mJ, resulting in a fluence below the damage threshold of the barium nitrate crystal yet large enough to saturate the single-pass Raman gain. This pump energy is optimized to maximize spectrum and mode profile rather than energy in this stage since the output energy of the six-pass Ti:sapphire amplifier is only weakly affected by seed energy. The 800-nm Raman pump passes through a delay stage to synchronize it with the seed pulse. Both pump and seed are sent to a Raman amplifier crystal, which is also barium nitrate. The two are overlapped in the amplifier crystal, and the pump and seed pulses are collimated with respective waists of  $w_p = 0.3$  cm and  $w_s = 0.25$  cm. As shown in Fig. 2, the seed and pump pulses are overlapped in the Raman amplifier with a noncollinear geometry, which utilizes four-wave mixing processes in addition to SRS to amplify the first Stokes' wave. The pump will arrive at a small ( $\sim 3.5$  deg) angle relative to the seed beam, in order to optimize phase matching for this latter process.

Pulse overlap in the Raman pump line is achieved by adjusting the pump line timing until the maximum energy output is achieved. Grigsby et al.<sup>12</sup> reported the observation of several side peaks at delay times of 10 and 30 ps, which were attributed to prepulses from the main 800-nm laser system. Our laser system uses cross-polarized wave generation to minimize such pulses with a contrast ratio of  $10^{10} : 1$ , which should therefore reduce or eliminate altogether these side peaks. However, we continue to observe such peaks, as shown in Fig. 3.

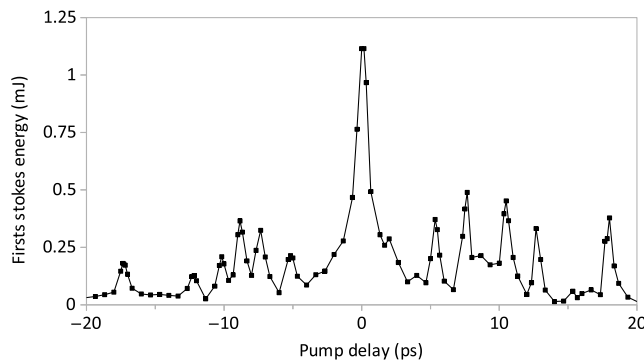


**Fig. 3** Second-stage Raman amplifier first Stokes pulse energy as a function of the pump pulse delay with respect to the seed pulse.

This amplified Raman beam is then used to seed a six-pass Ti:sapphire amplifier, which is externally pumped by a 1.1-J, 532-nm frequency-doubled Nd:YAG laser of FWHM 0.7 cm and top-hat transverse profile. An interference filter that is centered at 880 and with an FWHM bandwidth of 70 nm is used to remove any light at the fundamental frequency from the first Stokes signal. This is a safety precaution for the Ti:sapphire amplifier system, because the gain curve for Ti:sapphire is a factor of  $\sim 2$  greater at 800 nm than at 873 nm, and so any light at 800 nm will be preferentially amplified. The beam expands slightly through the cavity, from an initial waist size of 0.25 mm to a final size of 0.30 cm, which means that the fluence is sufficient to cause damage to the compressor gratings. Therefore, the beam is expanded and collimated at 4-cm FWHM in intensity.

This beam is then compressed by a 1200 lines/mm grating pair and sent to a target chamber, where it rejoins the main pulse via a dichroic mirror. Meanwhile, the main 800-nm pulse is passed through a delay line and then compressed to 25 fs, after which it is sent to the target chamber.

### 3 Results and Discussion

#### 3.1 Pulse Energy and Transverse Mode

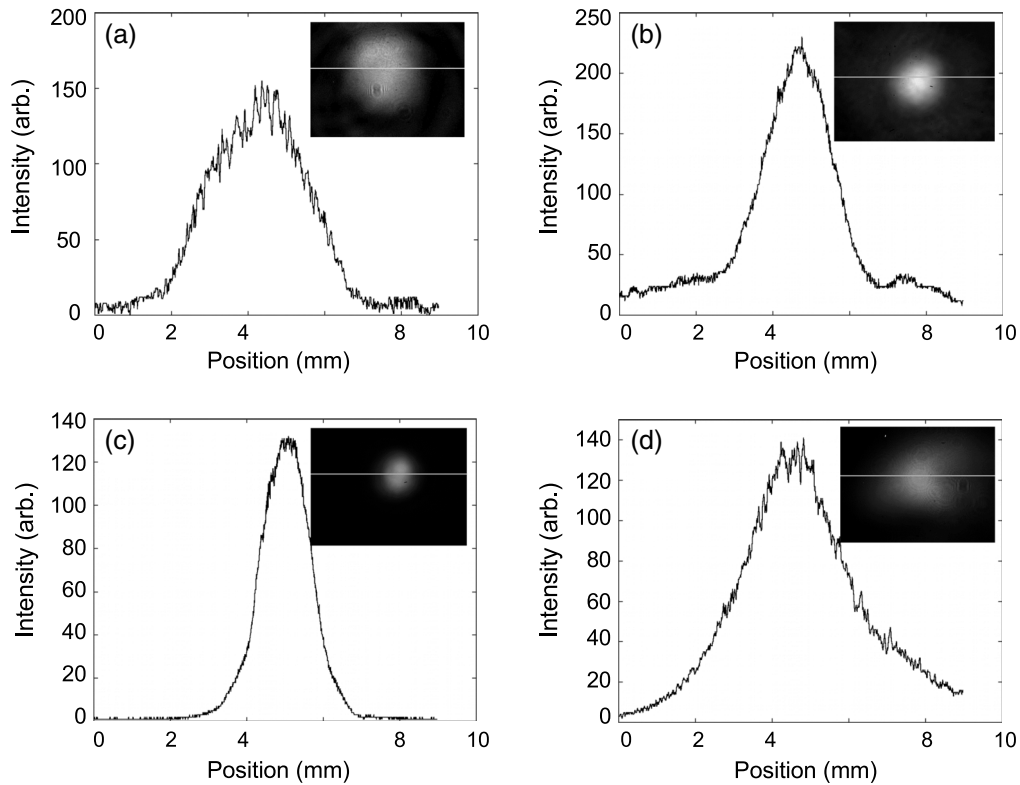
Typical second-stage single-pass energy yield is  $\sim 1.2$  mJ in the first Stokes' band. The higher order Stokes and anti-Stokes bands are also observed, and they are spatially separated from the first Stokes' signal due to the noncollinear geometry of the second stage.<sup>12,13,16</sup> Because the various Raman spectral bands and especially the residual fundamental laser at 800 nm would compete with the first Stokes band for gain in the Ti:sapphire amplifier, the second-stage output is filtered by a narrowband interference filter to select the first Stokes spectrum. This filter reduces the energy of the fundamental and all unwanted Stokes bands by  $>3$  orders of magnitude while reducing the energy of the desired first Stokes band by only  $\sim 30\%$ . Therefore, the third stage is typically seeded with 0.8 to 0.9 mJ of first Stokes' light.

Figure 4 shows the mode evolution in the far field, from the 800-nm pump beam (a) to the resulting Raman seed (b), which is then amplified and cleaned up (c) in the second-stage Raman amplifier, and then shaped by the pumping laser in the Ti:sapphire crystal (d). The Raman beam is cleaned up in the second stage due to the average effect of its overlap with the pump beam as both propagate through the second-stage amplifier crystal. Additionally, the mode structure out of the second-stage Raman amplifier crystals was such that only a part of the mode could be overlapped with the pump lasers in the Ti:sapphire crystal.

On one hand, the result of this is an improvement in the third-stage amplified mode as compared with the second-stage mode [Figs. 4(c) and 4(d)] and on the other hand, a lower energy yield. The Ti:sapphire gain was such that the  $\sim 1$ -mJ seed energy can be amplified to as much as  $\sim 300$  mJ after six passes [Fig. 5(b)] after the Ti:sapphire amplifier (but before compression), which is approximately half of the theoretical limit for a 1.1-J pump with 90% absorption. We observed energies of up to 310 mJ after amplification in the third stage [Fig. 5(a)], in good agreement with the simulations that account for losses on the system's mirrors [Fig. 5(b)]. In previous work,<sup>12</sup> which relied only on Raman amplification, a two-pass Raman amplifier was used to achieve a greater final energy ( $\sim 6$  mJ). However, the six-pass energy output from the Ti:sapphire amplifier is not especially sensitive to the seed energy generated by the second-stage amplifier. For example, doubling the seed energy from 1 to 2 mJ results in only about a 10% increase in final energy. Therefore, we are able to simplify the second-stage Raman amplifier by making only a single pass.

#### 3.2 Spectrum and Duration

Ideally, the amplified Raman pulse could be compressed to 25 fs to match the duration of the main 800-nm laser system, though some applications are more suited to a slightly stretched pulse.<sup>17</sup> Ultimately, pulse compression is limited by the bandwidth of the Raman signal. We observed gain narrowing from  $\sim 40$ -nm FWHM for the 800-nm signal to  $\sim 10$  to 15 nm after the second stage (typical) with some pulses as broad as 20 nm. This narrowing is due in part to



**Fig. 4** Evolution of the far field mode through the first three stages of the Raman CPA system. These show the horizontal lineouts of the mode, with the mode image itself as an inset. (a) The mode of the 800-nm fundamental beam as used to pump the amplifier crystal in the second stage. (b) The Raman signal used to seed this second stage (e.g., the signal out of the first stage) is somewhat bimodal, (c) but the beam undergoes some cleanup after one pass through the amplifier crystal in the second stage, and (d) is further cleaned up (and also shaped) in the Ti:sapphire crystal after six passes. The total energy in (d) is 105 mJ.

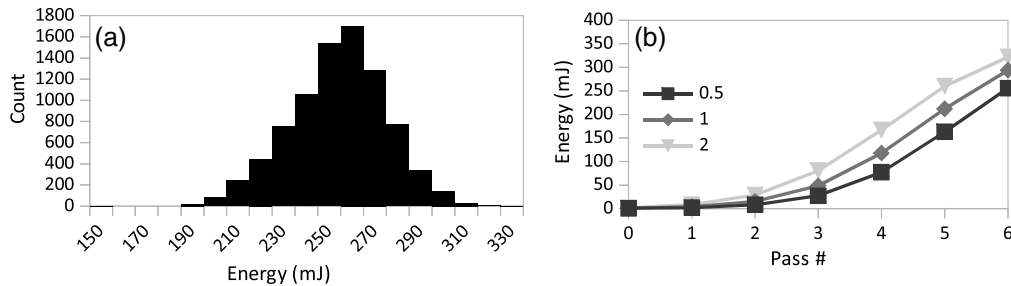


**Fig. 5** Energy output from the third-stage Ti:sapphire amplifier (before compression) for (a) six passes through the Ti:sapphire amplifier when pumped by a 1.1 J pulse, and (b) simulated after each of six passes and 1.1 J pump at 532 nm. The Raman beam has initial energies of 0.5 mJ (squares), 1.0 mJ (diamonds), and 2.0 mJ (triangles), and is assumed to have a 3% per-pass loss in the absence of the pump.

the depletion of the Raman gain for the trailing (blue) edge of the pulses. To achieve a broad bandwidth, the crystal must be driven hard enough for the frequency modes leading edge of the chirped pulse to experience SRS; however, when this happens the Raman gain in the crystals saturate, which causes the trailing edge of the pulses to have fewer Raman scatterings per mode, the result of which is both a redshifting of the Raman pulse itself and a narrowing of the pulse bandwidth.

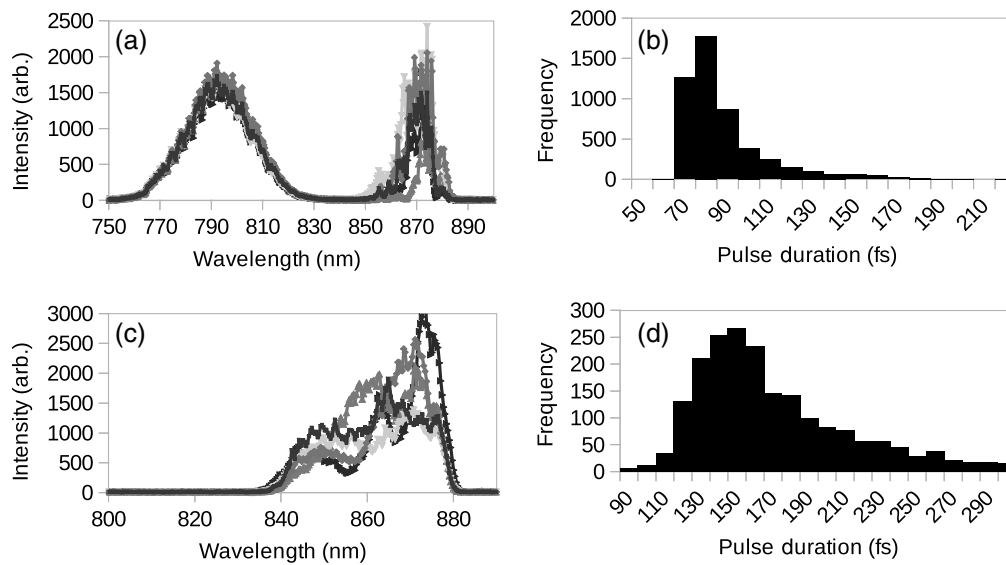


**Fig. 6** Spectra and pulse duration after compression for the beam output of the second and third stages. (a) The spectrum output from the Raman amplifier stage, superimposed on the fundamental spectrum. (b) Histogram of compressed pulse FWHM durations after Raman amplifier. (c) Output spectrum of the Raman laser after final amplification in the Ti:sapphire crystal. (d) Histogram of the compressed pulse duration after final amplification.

Figure 6 shows the spectra and pulse durations for the Raman laser. The second-stage spectra [Fig. 6(a)] are superimposed over the spectra of the 800-nm laser used to seed the first stage and pump the second stage of the Raman system. This superimposition was accomplished using a split-fiber spectrometer—two “input” sides to the fiber, one for the fundamental and one for the first Stokes signal—which merges into a single fiber input to the spectrometer. Different neutral-density filtering levels were used for each input, so the two are not to scale. Note that the first Stokes is centered around 873 nm for an incident pulse centered on 792 nm, whereas it should see a shift of  $\sim 73$  nm. If we increase the pump energy in the second stage, we observe that the spectrum shifts even more to the red and can shift by as much as  $\sim 90$  nm, resulting in a Raman pulse centered at 885 nm, which then has a typical bandwidth of  $\sim 5$ - to 10-nm FWHM. On the other hand, if the second-stage pump energy is decreased, then the spectrum will peak at the expected wavelength of 865 nm, but again with a relatively narrow bandwidth of  $\sim 10$ -nm FWHM (typical). The broadest pulses from the third stage have a bandwidth of  $\sim 15$  nm.

As noted by Grigsby et al.,<sup>12</sup> the Stokes shift breaks the symmetry between stretching and compression so that the 1480 lines/mm gratings used for the main laser system cannot be used to compress the Raman laser. Therefore, we used ray-tracing software (ZEMAX) as well as a Fourier transform routine in LABVIEW to simulate the compression of the Raman pulse for a 1200 line/mm grating pair. By setting the group-velocity dispersion and third-order dispersion to zero for the system with the stretcher, Raman shifter, and amplifier stages, and compressor to zero, we calculated the compressibility of the Raman laser system. According to these simulations, the 1200 lines/mm gratings will compress the first Stokes’ pulse to near the bandwidth limit (assuming an approximate Gaussian pulse) with a grating separation distance of 54.97 cm and an incident angle of 38.2 deg. This corresponds to a  $\sim 75$ -fs pulse with a 15-nm FWHM spectrum [Fig. 7(a)]. Actual compressed pulse durations were measured using a single-shot autocorrelator [Fig. 7(b)].

Typical pulse durations after the Raman amplifier were 95 to 100 fs, with pulses as short as 75 fs. These pulse durations achieved were near the bandwidth limit for a Gaussian pulse and represent an improvement to the pulse durations achieved in previous experiments, which is due to a broader bandwidth than was observed by Zhavoronkov et al.<sup>11</sup> or Grigsby et al.<sup>12</sup> However, the presence of prepulses or pulse pulses in the pumping laser can cause the broadening of these pulse durations or generate prepulses and postpulses in the final compressed Raman beam, as shown by Chen et al.<sup>18</sup> The further gain narrowing of the spectrum in the Ti:sapphire amplifier

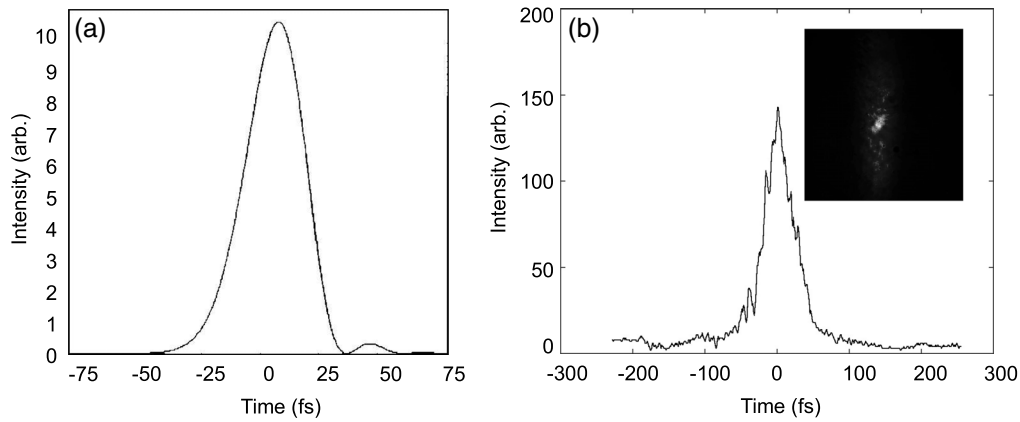


**Fig. 7** Autocorrelation traces for the compressed Raman laser. The compressed pulse was simulated (a) for the 1200 lines/mm grating compressor assuming spectral narrowing to 15-nm FWHM, and (b) the corresponding second-order correlation trace with single-shot autocorrelation image inset.

results in an increase of the pulse durations, with the shortest pulses being 90 to 100 fs and typical pulses being 140 to 150 fs in duration when fully amplified and then compressed.

The energy loss on the compressor grating pair is ~40%. Thus, the compressed pulse energy is 140 mJ at 140 fs—that is, ~1.0 TW. However, powers up to ~2 TW have been realized.

### 3.3 Focus and Intensity

The final mirror before target is replaced by a wedge that reflects ~96% of the beam to target and transmits the remaining ~4% for diagnostic purposes. This allows for *in-situ* diagnostics to be run for the beam, including beam profile (and pointing) at focus. The focal plane is relay-imaged: the beam is actually focusing when reflected from a mirror, so it is first collimated using one lens and then focused using an identical lens, with a 20× microscope objective placed near the relayed focus and used to image the focal plane onto a CCD camera. An interference filter can then be used to distinguish between fundamental and first Stokes beams; the profiles of these two beams are shown in Fig. 8. The size can then be calibrated using an USAF test pattern target, placed at the beam’s relayed focus.

The size of the first Stokes beams at focus is  $10.6 \pm 0.2 \mu\text{m} \times 16.2 \pm 0.7 \mu\text{m}$ , as compared with  $8.8 \pm 0.2 \mu\text{m} \times 11.1 \pm 0.9 \mu\text{m}$  for the fundamental beam. It should be noted that the reason for a larger focal spot for the Raman beam at focus is that the far field beam size is limited to only 5 cm so as to not clip in optical gratings, whereas the fundamental beam’s far field size can be somewhat larger due to a larger pair of gratings.

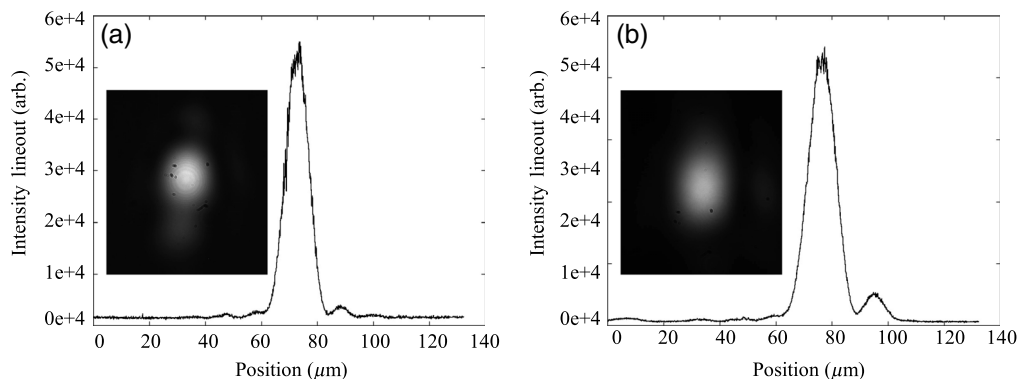


**Fig. 8** Relay-imaged beam focus profile intensity lineouts for (a) fundamental and (b) first Stokes beams, with insets images of the transverse modes at focus.

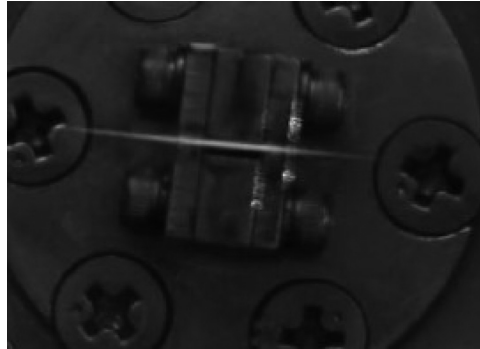


**Fig. 9** Ionization spark trail in air caused by the ionization of primarily nitrogen atoms in the air. The gas jet in this image is also the target gas jet and measures  $3 \text{ mm} \times 1 \text{ mm}$ , and can be used to approximate scale.

The intensity of the first Stokes beam is measured in one of three ways: by simple calculation, by air-ionization trail length, or by ionization threshold in vacuum. The peak intensity of a Gaussian beam of spot waist  $w_0$ , duration  $\tau_L$ , and pulse energy  $W$  is

$$I_{\text{peak}} \approx \frac{2W}{\pi\tau_L w_0^2}. \quad (1)$$

This calculation yields a peak intensity of  $1.4 \times 10^{17} \pm 7 \times 10^{16} \text{ W/cm}^2$ , where the fluctuation is calculated as the standard deviation over thousands of shots and is primarily due to fluctuations in beam energy and duration. The other two measurements are based on a method developed for use in laser-plasma interactions,<sup>19</sup> in which the intensity of the laser pulse is determined by its ability to ionize a known gas via barrier suppression.<sup>20</sup> Essentially, we use the threshold for barrier-suppression ionization in helium or air to estimate the intensity of the laser. An image of the air-ionization “spark trail” is shown in Fig. 9.

The leading edge of this trail represents the location at which the beam’s intensity exceeds barrier-suppression intensity ( $I_{\text{BS}}$ ) at which ionization occurs. This occurs before the focus, but a simple comparison of the spot sizes at this ionization threshold ( $w_{\text{ion}}$ ) and at the focal plane of the beam in vacuum ( $w_0$ ) yields the peak intensity:

$$I_{\text{peak}} \approx \frac{w_{\text{ion}}^2}{w_0^2} I_{\text{BS}}. \quad (2)$$

This method gives a beam intensity of  $3.8 \times 10^{17} \pm 9 \times 10^{16} \text{ W/cm}^2$ ; the discrepancy between this and other measurement and calculation values is due to the presence of other atomic species in air and to the fact that some ionization may occur via tunneling.

The third method used to determine on-shot intensity utilizes a gas jet (Fig. 9) under vacuum. The gas jet is mounted on a three-axes translation stage. It is translated until the threshold ionization position for helium gas jet is found, both before and after the beam’s focus.

Since the position of this threshold and therefore the beam’s waist is known, the intensity can be determined as in the previous method, yielding a peak intensity of  $1.12 \times 10^{17} \pm 4 \times 10^{15} \text{ W/cm}^2$ . While shorter Raman-shifted pulse durations have been realized,<sup>21</sup> these are the highest energy and intensity pulses generated by this method.

The fundamental beam has a nominal intensity of  $3 \times 10^{19} \text{ W/cm}^2$ , as specified by the manufacturer.

## 4 Conclusion

We have built a two-color TW laser system by adding a Raman-shifted second color to a conventional 45-TW Ti:sapphire laser. This second color does not diminish the performance of the main laser system. We have observed reasonable stable mode and pointing-on-target pulses, which are amplifiable to  $>200 \text{ mJ}$  before compression. The bandwidth undergoes some narrowing not

previously observed for narrower ( $\sim 10$  nm FWHM) systems, which is due to the depletion of the Raman gain by the leading edge of the 800-nm seed/pump pulses. However, the bandwidth is still sufficient to allow pulses to be compressed to  $<100$  fs. We have therefore demonstrated that the Raman shifting process can be amplified to TW powers for the creation of a two-color TW laser system. These pulses are sufficiently strong to be used in two-color pump–probe experiments, as demonstrated by a simple ionization detection experiment in which either pulse may be used to defocus the other pulse via ionization defocusing.

## Acknowledgments

We thank Franklin Grigsby for his advice during early stages of this experiment, and Spencer Jolly for his help in preparation during latter parts of the experiment. Funding for this research was provided by U.S. Department of Energy Grant DE-SC0011617 and the Air Force Office of Scientific Research Grant FA9550-16-1-0013.

## References

1. R. Zgadzaj et al., “Femtosecond pump–probe study of preformed plasma channels,” *J. Opt. Soc. Am. B* **21**(8), 1559–1567 (2004).
2. G. Shvets et al., “Superradiant amplification of an ultrashort laser pulse in a plasma by a counterpropagating pump,” *Phys. Rev. Lett.* **81**, 4879–4882 (1998).
3. S. Kalmykov and G. Shvets, “Compression of laser radiation in plasmas using electromagnetic cascading,” *Phys. Rev. Lett.* **94**(23), 235001 (2005).
4. H. Hora, “Theory of relativistic self-focusing of laser radiation in plasmas,” *J. Opt. Soc. Am.* **65**(8), 882–886 (1975).
5. S. Kalmykov, S. Yi, and G. Shvets, “All-optical control of nonlinear focusing of laser beams in plasma beat wave accelerator,” *Plasma Phys. Control. Fusion* **51**(2), 024011 (2009).
6. S. Kalmykov, S. Yi, and G. Shvets, “All-optical suppression of relativistic self-focusing of laser beams in plasmas,” *Phys. Rev. E* **78**(5), 057401 (2008).
7. M. Fomyts’kyi et al., “Controlled plasma wave generation and particle acceleration through seeding of the forward Raman scattering instability,” *Phys. Plasmas* **12**, 023103 (2005).
8. T. Tajima and J. Dawson, “Laser electron accelerator,” *Phys. Rev. Lett.* **43**(4), 267–270 (1979).
9. W. P. Leemans et al., “GeV electron beams from a centimetre-scale accelerator,” *Nat. Phys.* **2**, 696–699 (2006).
10. I. Blumenfeld et al., “Energy doubling of 42 GeV electrons in a metre-scale plasma wake-field accelerator,” *Nature* **445**, 741–744 (2007).
11. N. Zhavoronkov et al., “Chirped-pulse stimulated Raman scattering in barium nitrate with subsequent recompression,” *Opt. Lett.* **26**(1), 47–49 (2001).
12. F. Grigsby, P. Dong, and M. Downer, “Chirped-pulse Raman amplification for two-color, high-intensity laser experiments,” *J. Opt. Soc. Am. B* **25**(3), 346–350 (2008).
13. X. Guo et al., “Chirped pulse Raman amplification in  $\text{Ba}(\text{NO}_3)_2$  crystals,” *Opt. Laser Technol.* **67**, 8–11 (2015).
14. T. T. Basiev et al., “Raman spectroscopy of crystals,” *Opt. Mater.* **11**, 307–314 (1999).
15. T. T. Basiev et al., “Comparative spontaneous Raman spectroscopy of crystals for Raman lasers,” *Appl. Opt.* **38**, 594–598 (1999).
16. Y. Xu et al., “Raman amplification to generate picosecond laser pulses in  $\text{YVO}_4$  crystal,” *Lasers Eng.* **30**(5/6), 363–368 (2015).
17. S. Y. Kalmykov, B. A. Shadwick, and M. C. Downer, “All-optical control of nonlinear self-focusing in plasmas using non-resonantly driven plasma wave,” in *AIP Conf. Proc. Adv. Accel. Conc. 14*, Vol. CP1299, 752–759 (2010).
18. J. Chen et al., “Investigation of pre-pulse pumping laser for preserving temporal waveform of stimulated Raman scattering,” *Laser Phys.* **27**, 015402–015408 (2017).
19. A. Link et al., “Development of an in situ peak intensity measurement method for ultra-intense single-shot laser-plasma experiments at the Sandia Z petawatt facility,” *Rev. Sci. Instrum.* **77**(10), 10E723 (2006).

20. M. Amosov and N. Delone, "Tunnel ionization of complex atoms and atomic ions in electromagnetic field," *Proc. SPIE* **0664**, 138–140 (1986).
21. N. V. Didenko et al., "40-fs hydrogen Raman laser," *Quantum Electron.* **45**(12), 1101–1104 (2015).

**James C. Sanders** is an assistant professor in the Department of Chemistry and Physics, Troy University. He received his HBS in physics from Oregon State University in 2006, and his PhD degree in physics from the University of Texas at Austin. His current research interests include MIE scattering, remote sensing, and physics education research with an emphasis on undergraduate student projects.

**Rafal Zgad Zaj** earned his PhD from the University of Texas at Austin, where he is currently a research scientist. He has also conducted research at the Brookhaven National Laboratory, SLAC National Laboratory, and the Helmholtz-Zentrum Dresden-Rossendorf, Germany. His work focuses on the physics of laser driven and electron beam driven plasma accelerators, associated generation of x-ray radiation, as well as related advanced diagnostics of plasma structure, electron beams, and high energy x-rays.

**Michael C. Downer** earned his PhD in 1983 from Harvard University, and is now professor of physics and distinguished university teaching professor at the University of Texas at Austin, where he has supervised 42 PhD and 23 MS dissertations on topics ranging from laser-plasma particle accelerators to optical spectroscopy of surfaces. He is a fellow of the American Physical Society and OSA, and a 2016 Humboldt Research Prize winner.